



## Article

# Investigation on Vertical Position and Sound Velocity Variation for GNSS/Acoustic Seafloor Geodetic Calibration Based on Moving Survey Data

Rui Shan <sup>1,2</sup>, Huimin Liu <sup>2,\*</sup>, Shuang Zhao <sup>3,4</sup>  and Haojun Li <sup>1</sup><sup>1</sup> College of Surveying and Geo-Informatics, Tongji University, 1239 Siping Road, Shanghai 200092, China<sup>2</sup> Qingdao Institute of Marine Geology, China Geological Survey, 596 Guanshan Road, Qingdao 266237, China<sup>3</sup> Chinese Academy of Surveying & Mapping, 28 Lianhuachi West Road, Beijing 100036, China<sup>4</sup> Institute of Industrial Science, University of Tokyo, 4-6-1 Komaba, Tokyo 153-8505, Japan

\* Correspondence: liuhuimin@mail.cgs.gov.cn; Tel.: +86-1876-5922-885

**Abstract:** The accuracy of GNSS/Acoustic seafloor geodetic calibration is greatly influenced by the temporal variation of sound velocity, especially in the vertical direction. Aiming at correcting of the unknown parameters related to both the positions and the sound velocity, this paper proposes a step-by-step inversion scheme based on moving survey data. The proposed method firstly estimates the horizontal normalized travel time delay with sound ray tracing strategy and then computes the horizontal position with circle line observations. We reconstructed an inversion scheme for extracting the surface sound velocity disturbance (SSVD) and corrected the vertical position from cross line data. The SSVD is decomposed into a sum of different period disturbances, and a new SSVD is reconstructed by combining the long period disturbance and short period disturbance. The proposed algorithm is verified by the South China Sea experiment for GNSS/Acoustic seafloor geodetic calibration. The results demonstrate that the new method can take the effects of sound velocity variation into consideration and improve the precision of the vertical position, which is superior to the least squares (LS), the single-difference LS for seafloor geodetic calibration.

**Keywords:** GNSS/Acoustic; seafloor geodetic calibration; sound ray tracing; surface sound velocity disturbance; vertical position



**Citation:** Shan, R.; Liu, H.; Zhao, S.; Li, H. Investigation on Vertical Position and Sound Velocity Variation for GNSS/Acoustic Seafloor Geodetic Calibration Based on Moving Survey Data. *Remote Sens.* **2022**, *14*, 3739. <https://doi.org/10.3390/rs14153739>

Academic Editors: Yusuke Yokota and Takumi Matsuda

Received: 30 June 2022

Accepted: 2 August 2022

Published: 4 August 2022

**Publisher's Note:** MDPI stays neutral with regard to jurisdictional claims in published maps and institutional affiliations.



**Copyright:** © 2022 by the authors. Licensee MDPI, Basel, Switzerland. This article is an open access article distributed under the terms and conditions of the Creative Commons Attribution (CC BY) license (<https://creativecommons.org/licenses/by/4.0/>).

## 1. Introduction

The GNSS/Acoustic (GNSS/A) technique was devised in the 1980s [1], which is a combination technique of kinematic GNSS positioning and underwater acoustic ranging for seafloor geodetic absolute positioning. Since the seafloor geodetic benchmarks for detecting absolute seafloor crustal deformations were established, it has yielded many significant results, including detection of interseismic [2,3], coseismic [4,5], and postseismic deformation associated with earthquake [6,7], as well as plate motions [8–11]. However, the positioning service or deformation analysis using the seafloor benchmarks is affected by the accuracy of locations of seafloor benchmarks. Thus, it is necessary to improve the accuracy of the seafloor geodetic absolute calibration and realize efficient observations.

The observation accuracy of GNSS/A is mainly limited by the acoustic ranging error, especially caused by the temporal fluctuations of sound velocity within the observation period [12–14]. In general, the sound velocity is generally assumed to be vertically stratified in seawater with the underwater acoustic signals conforming to Snell's law. By adopting the sound ray-tracing (SRT) strategy based on the sound velocity profiles (SVPs) data, the propagation paths of acoustic signals can be tracked [15,16]. The sound velocity is not only affected by seasonal and daily variations in ocean conditions but also by more detailed temporal and spatial variations caused by several factors such as internal waves, anomalous temperature and water masses [17]. There are difficulties for the SVP data

to balance real-time and accurate demands due to the time fluctuation of sound velocity within tens of minutes to a few hours, especially during moving calibration surveys. As for GNSS/A absolute calibration observation, the single transponder is positioned by controlling the vessel sailing around a circle with a nominally constant radius [18,19]. The surveying strategy is effective in precisely determining the horizontal components of the center transponder, since systematic errors have been cancelled out [2,20]. However, the accuracy of vertical components remains difficult to improve, limited by the sound velocity temporal variation, especially surface sound velocity disturbance [21].

Many previous GNSS/A studies have proposed several methods to correct the effect of sound velocity variation. Osada et al. succeeded in estimating the temporal variation of sound velocity from acoustic data [22]. Xu et al. proposed a single difference (SD) method for single point seafloor positioning and the double difference method for relative seafloor positioning to remove the effect of systematic errors [13]. The simulations have shown that the accuracy of single point positioning can be determined with one centimeter in the three dimensions, and the performance remains to be further validated using the field data. When the reference sound velocity profile is different from the actual profile, it ultimately affects the discrepancy between the estimation of the propagation time delay. Fujita et al. removed this effect by using a simple time function to estimate the temporal variation of the acoustic velocity structure [14]. The results showed that the temporal and spatial stability of the acoustic velocity structure in the seawater depend on the region and season. Kido et al. proposed a generalized expression of sound velocity variation in terms of a travel time residual normalized to the vertical component to acoustically estimated sound velocity [23]. This method also provides a reference for many future studies [2,5,7,24,25]. Chen et al. estimated the relative positions of three transponders and a constant sound velocity bias by an optimization technique combined with ray-tracing calculations [26]. The results show that the accuracy of relative positioning is insensitive to the surface sound velocity disturbance at a depth of 300 m. In the last ten years, analytical procedures with the estimation of the spatial sound velocity gradient for the moving-around pattern have been developed. Yokota et al. proposed a technique for extracting the gradient effects of sound velocity structure through multiple modeling [3]. Honsho et al. showed a more general expression for one-directional sound velocity gradient, and the accuracy of the seafloor positioning was also improved by the above inversion scheme [7]. However, most of those studies have basically adopted the Scripps Institution of Oceanography (SIO) approach [1], which locates a virtual geodetic station and estimates the sound velocity variation using the transponders array. In GNSS/Acoustic seafloor geodetic absolute calibration, each seafloor transponder is an independent geodetic station [27], and the influence of sound velocity variation on ranging error is intuitively related to various factors such as propagation time, incidence angle and depth, which increase the complexity of data processing.

There are two key points involved in vertical positioning and sound velocity variation. One is the observation configuration optimization that can be constructed by designing different survey lines and the array of seafloor stations, and the other is to determine the appropriate inversion scheme for solving the optimization problem. As for the data post-processing, the observation configuration has been determined. Thus, we focus on the improvement of the inversion scheme. In this contribution, the step-by-step inversion scheme has been proposed to simplify the difficulty of parameter estimation and to improve the positioning accuracy in the vertical direction based on the moving survey data. Furthermore, in the experiment, the cross-survey lines over the top of the transponder are arranged. In order to improve the vertical accuracy and estimation efficiency of the absolute positions of the seafloor reference stations, we performed a vertical position inversion and sound velocity perturbation inversions iteratively to obtain the final solutions from cross line data. Finally, we discuss our results on the South China Sea experiment.

## 2. Principles of the GNSS/Acoustic Seafloor Geodetic Move-Around Calibration Method

### 2.1. Observation System

A conceptual model of the seafloor absolute calibration system is shown in Figure 1, which refers to the process of transferring positioning from a surface positioning system referenced to a global reference frame to a seafloor transponder. This typically involves the simultaneous observation of the GNSS positioning and the attitudes of a vessel while acoustically ranging toward the fixed seafloor transponder from a transducer and known offsets from the GNSS antenna on the vessel. A single transponder is positioned by controlling the vessel sailing around a circle with a nominally constant radius to remove systematic errors. By collecting geometrically symmetric data, the positioning accuracy and observation efficiency tend to be improved [28–31]. In order to ensure geometric structure of the observation, the radius of the circle that the surveying vessel sails around is approximately 50% to 150% of the water depth. The distance between the seafloor transponder and the vessel transducer is estimated by acoustic round-trip traveling time.

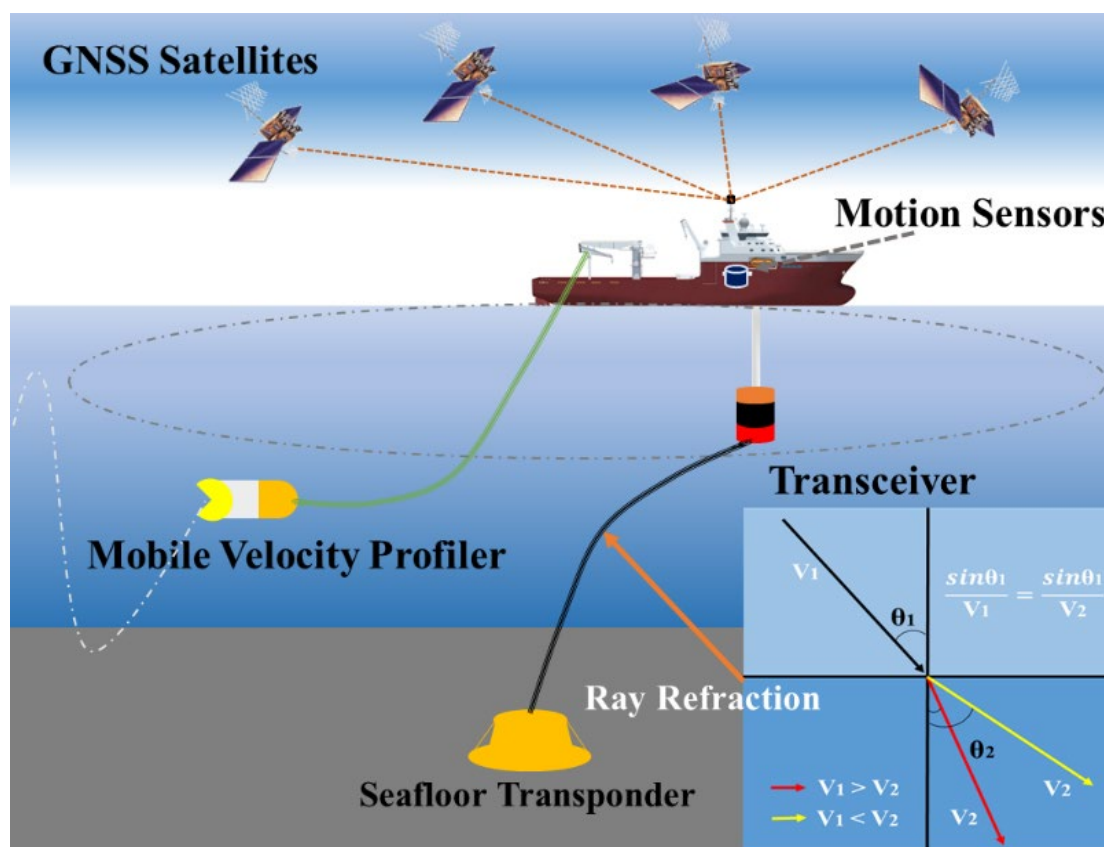


**Figure 1.** Schematic of the GNSS/Acoustic seafloor geodetic observation system.

The sound velocity can be measured by a velocimetry or computed from measurements of the water temperature, salinity and pressure using a conductivity temperature depth (CTD) profiler [32]. However, the temperature varies significantly with time and space, particularly in shallow parts, and the accuracy of the sound velocity is limited by the empirical equations that relate these parameters to sound velocity.

### 2.2. Basic Ray-Tracing Strategy for GNSS/Acoustic Absolute Calibration

The basic principles of the GNSS/Acoustic absolute calibration during an interrogation/reply cycle are shown in Figure 2a. When the vessels steam around a circle, the location of the vessels is changed, and the round-trip traveling time for interrogation and reply must be calculated separately.

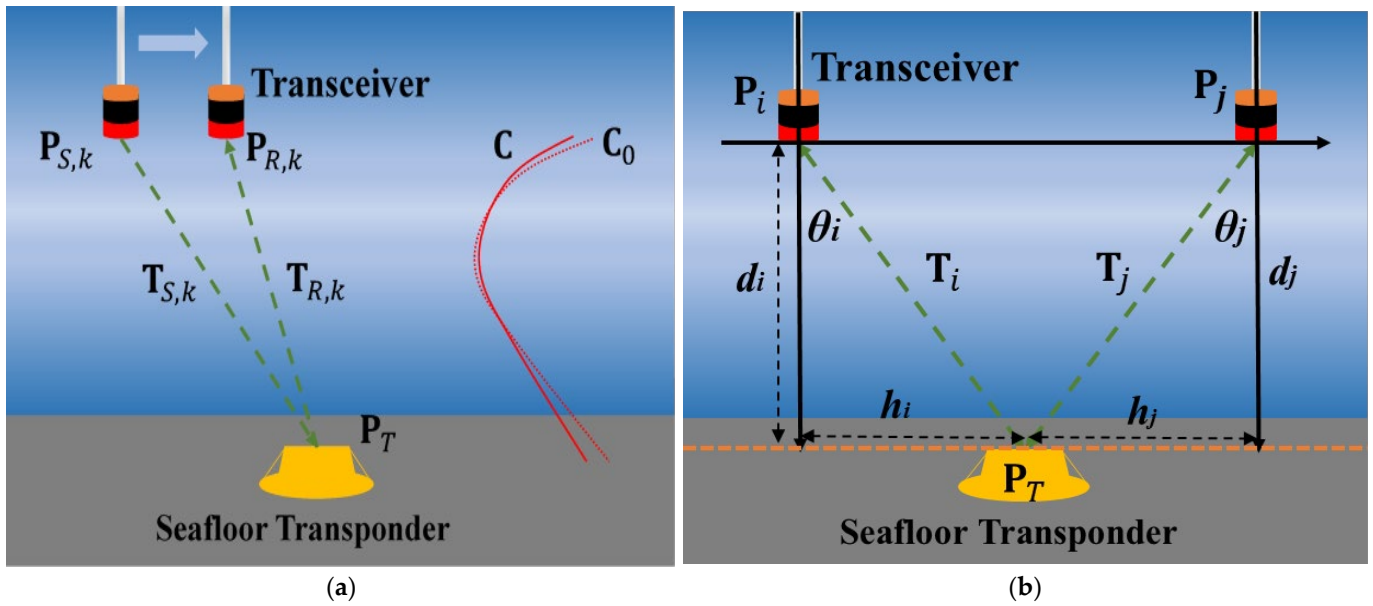


**Figure 2.** The round-trip acoustic travel time for one interrogation–reply cycle (a). The geometry scheme of transducer and transponder  $i$  and  $j$  stand for different observation cycles (b).

Assuming a laterally stratified sound velocity structure, to estimate the transponder position  $P_T = [X_T \ Y_T \ Z_T]$  precisely, let  $P_{S,k} = [X_{S,k} \ Y_{S,k} \ Z_{S,k}]$  be the positions of the transceiver at the time of sending and  $P_{R,k} = [X_{R,k} \ Y_{R,k} \ Z_{R,k}]$  be the positions of the transceiver at the time of receiving acoustic signals. The observation equation expressing the round-trip travel time for the seafloor transponder at time  $k$  is represented as:

$$T_{m,k} = T_{S,k} + T_{R,k} + \varepsilon_k \quad (1)$$

with

$$T_{S,k} = f(P_T, P_{S,k}, C_k), \quad T_{R,k} = f(P_T, P_{R,k}, C_k) \quad (2)$$

where  $T_{m,k}$  represents the measured round-trip acoustic travel time. As shown in Figure 2a, the one-way travel time  $T_{S,k}$ ,  $T_{R,k}$  can be calculated using the ray-tracing technique with sound velocity profile  $C$  based on Snell's law.  $\varepsilon_k$  represents the random timing error.

The error equation of round-trip travel time can be expressed as:

$$V_k = T_{m,k} - f(P_{T,\rho}, P_{S,k}, C_0) - f(P_{T,\rho}, P_{R,k}, C_0) - \Delta T_{P,k} - \Delta T_{C,k}, \quad (3)$$

$$\Delta T_{P,k} \approx f(P_T, P_{S,k}, C_k) + f(P_T, P_{R,k}, C_k) - f(P_{T,\rho} + \delta P_T, P_{S,k}, C_k) - f(P_{T,\rho} + \delta P_T, P_{R,k}, C_k), \quad (4)$$

$$\Delta T_{C,k} \approx f(P_T, P_{S,k}, C_k) + f(P_T, P_{R,k}, C_k) - f(P_T, P_{S,k}, C_0 + \delta C_k) - f(P_T, P_{R,k}, C_0 + \delta C_k), \quad (5)$$

where  $P_{T,\rho}$  represents the initial transponder position,  $C_0$  represents the reference sound velocity profile,  $\Delta T_{P,k}$  and  $\Delta T_{C,k}$  denote the ray-tracing time error by position basis  $\delta P_T$  and sound velocity temporal variation  $\delta C$ , respectively.

The error sum of squared errors between the measured and calculated travel times is written as follows:

$$J(\delta P_T, \delta C_k) = \sum_{k=1}^n V_k^2, \quad (6)$$

where  $n$  is the number of acoustic observation pairs. When the average sound velocity along the actual ray path is expressed as  $C_m$ , the Euclidean distances and the transceiver and the transponder position can be calculated with the least square (LS) method; see Appendix A.

Kido et al. represented the temporal variation of sound velocity as a vertically normalized time delay relative to that for a reference model [23], which is called the Nadir Total Delay (NTD) [24].

Using the mapping function, the horizontal and vertically normalized travel time delay can be represented as follows:

$$\delta T_{H,k} = T_{m,k} \frac{2 \sin(\theta_{S,k}) \sin(\theta_{R,k})}{\sin(\theta_{S,k}) + \sin(\theta_{R,k})} - T_{S,k} \sin(\theta_{S,k}) - T_{R,k} \sin(\theta_{R,k}), \quad (7)$$

$$\delta T_{V,k} = T_{m,k} \frac{2 \cos(\theta_{S,k}) \cos(\theta_{R,k})}{\cos(\theta_{S,k}) + \cos(\theta_{R,k})} - T_{S,k} \cos(\theta_{S,k}) - T_{R,k} \cos(\theta_{R,k}), \quad (8)$$

where the travel-time delay  $\delta T_{H,k}$  and  $\delta T_{V,k}$  normalized by the mapping function are independent of the vertical and horizontal distance of the transducer, respectively.

Note that, if the sound velocity perturbation  $\delta c$  is a constant bias, based on the geometric symmetry of a circular track, the horizontal travel-time residual  $\delta T_{H,k}$  has a smaller effect on horizontal positioning. Meanwhile, the vertically travel-time residual normalized by the mapping function is independent of the horizontal distance of the transducer [33]. As shown in Figure 2b, if the depth error  $\delta d$  exists, the vertically travel-time residual normalized by the mapping function varies depending on the horizontal distance from the transducer to the transponder. The vertically normalized travel time delay can be represented as follows:

$$\delta T_{V,i} \approx \frac{d_i}{\sqrt{h_i^2 + d_i^2}} \left( \frac{\sqrt{h_i^2 + (d_i + \delta d)^2}}{C + \delta c} - \frac{\sqrt{h_i^2 + d_i^2}}{C} \right), \quad (9)$$

According to the Equation (9), the vertically normalized travel time delay includes not only information on the range, but also that on the velocity structure along the path. This also indicates that the sound velocity error and the depth error cannot be distinguished from the same incident angles for the transponders. Other observations with different indicant angles are essential to precisely estimate vertical displacements. During the acoustic absolute calibration, the sound velocity variation function  $\delta c$  is usually given as a simple time function.

### 3. Inversion Scheme

#### 3.1. Absolute Horizontal Position Estimation

In this research, the horizontal and vertical position are estimated to utilize a step-by-step method for moving survey data. We design two kinds of calibration survey lines, as shown in Figure 3: one is the circular line (Figure 3a), the other is the cross line (Figure 3b).

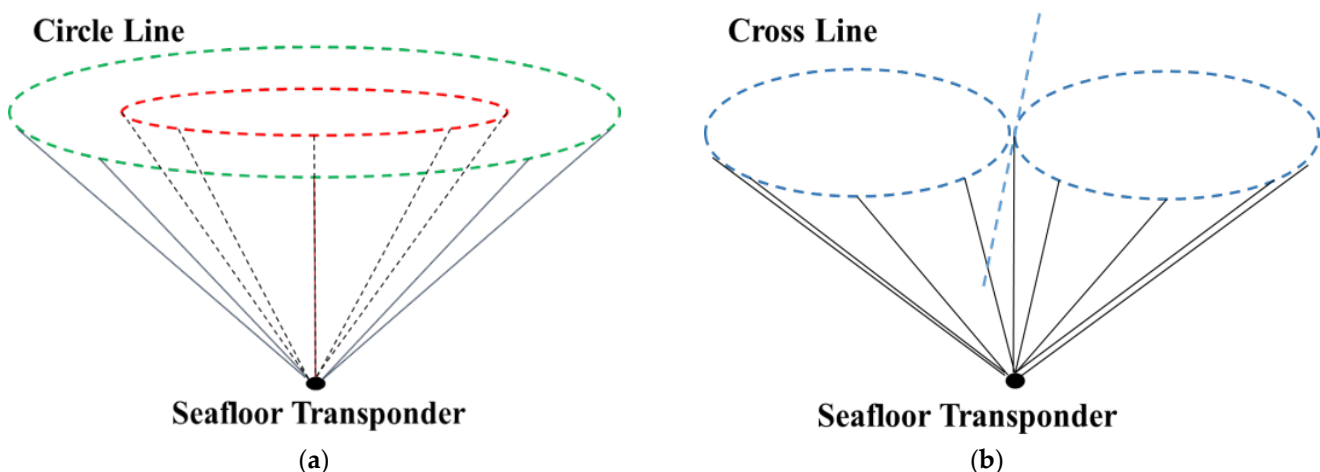


**Figure 3.** Calibration survey line. Two circles around the seabed transponder (a). A figure eight with the seabed transponder in the center (b).

In this research, these two types of survey lines are used to calculate the horizontal (2D) and vertical coordinates of the seabed reference station, respectively. As the LS method with circular calibration trajectory is insensitive to the sound velocity perturbation, it is possible to calculate the precision horizontal position precisely. The horizontal position can be used as the constraint to estimate the vertical position and the surface sound velocity disturbance (SSVD). The unknown

horizontal position can be estimated by solving the nonlinear Equation (7) for all circle line travel time data using the iterative least squares method. The nonlinear equation is locally linearized as follows:

$$\begin{aligned} \delta T_{H,k}^{Circle} &= \left[ \frac{\sin \theta_{S,k} \delta f_S}{\delta X_T} |X_{T,o} + \frac{\sin \theta_{R,k} \delta f_R}{\delta X_T} |X_{T,o} \frac{\sin \theta_{S,k} \delta f_S}{\delta Y_T} |Y_{T,o} + \frac{\sin \theta_{R,k} \delta f_R}{\delta X_T} |X_{T,o} \right] \begin{bmatrix} \delta X_T \\ \delta Y_T \end{bmatrix} \\ &= \left[ \frac{\kappa_{S,k} \sin \theta_{S,k} (X_{T,o} - X_{S,k})}{H_{S,k}} + \frac{\kappa_{R,k} \sin \theta_{R,k} (X_{T,o} - X_{R,k})}{H_{R,k}} \frac{\kappa_{S,k} \sin \theta_{S,k} (Y_{T,o} - Y_{S,k})}{H_{S,k}} + \frac{\kappa_{R,k} \sin \theta_{R,k} (Y_{T,o} - Y_{R,k})}{H_{R,k}} \right] \begin{bmatrix} \delta X_T \\ \delta Y_T \end{bmatrix} \end{aligned} \quad (10)$$

where  $\kappa_{S,k}$  and  $\kappa_{R,k}$  are sending and receiving Snell's constant and are computed by the ray-tracing.  $H_{S,k} = \sqrt{(X_{T,o} - X_{S,k})^2 + (Y_{T,o} - Y_{S,k})^2}$ , and  $H_{R,k} = \sqrt{(X_{T,o} - X_{R,k})^2 + (Y_{T,o} - Y_{R,k})^2}$ .

The observations of different incident angles through different cross lines are sensitive to vertical deviation and sound velocity disturbance. Thus, this observation pair also provides basis information for the inversion of coupled surface sound velocity disturbances and vertical deviations. To estimate the vertical position, it is necessary to find the best  $\delta Z_T$  and  $\delta C_k$  to minimize the following objective function:

$$J(\delta Z_T, \delta C_k) = \sum_{k=1}^n \delta T_{V,k}^2 \quad (11)$$

### 3.2. Surface Sound Velocity Temporal Variation Extraction Method

The absolute position of a transponder and temporal sound velocity variation can be estimated by finding the best values to minimize Equation (6). A variety of effective optimization algorithms, e.g., Bayesian least squares inversion [14], numerical optimization approach [26], linearized inversion method [3], extended Kalman filter [33], one step approach [7], are developed with different kinds of temporal sound velocity variation. In order to improve the vertical accuracy and estimation efficiency of the absolute calibration position, we performed a vertical position and sound velocity perturbation inversions iteratively to obtain the final solutions. The sound velocity perturbation inversion method was developed by Fujita et al. [14]. The shape of the vertical profile is also assumed to be invariable with time. Different from Fujita's method, for the absolute correction of a single transponder, this study only calculates the surface sound velocity disturbance (SSVD).

As shown in Figure 4, the reference sound velocity profile is divided into two parts: the shallow water area and the deep water area. Our method takes into account the shallow water sound velocity disturbances affected by the outside environment and reduces the number of inversion parameters. Consider that the surface sound velocity disturbance  $\delta C_k(z)$  varies in time with depths shallower than  $Z_{Surface}$ , then  $\delta C_k(z)$  can be rewritten as the sum of intrinsic model functions (IMFs)  $u$  and residual  $r$ :

$$\delta C_k(z) = \begin{cases} r_m(k) + \sum_i^m u_i(k) & (z \leq Z_{Surface}) \\ 0 & (z > Z_{Surface}) \end{cases}, \quad (12)$$

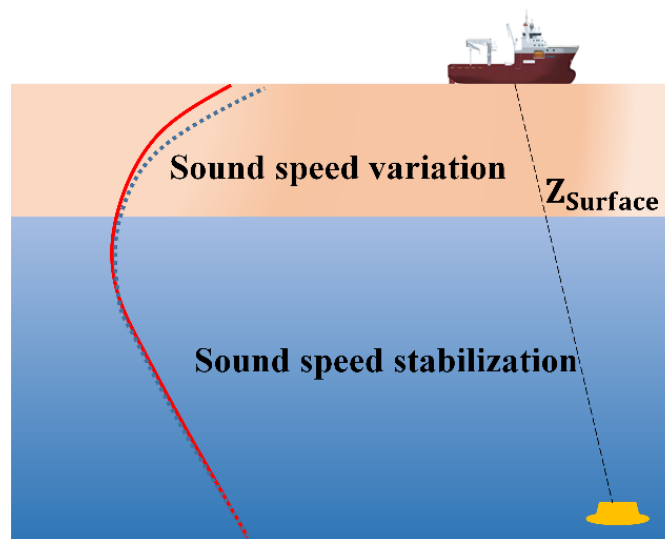


Figure 4. The scheme of sound velocity variation and stabilization.

Another important step is to calculate the  $\delta C_k(z)$  based on vertically normalized travel time delay  $\delta T_V$  and SRT method. In this study, the  $\delta C_k$  is calculated using the following SSVD extraction method (Algorithm 1).

---

**Algorithm 1** Surface sound velocity variation extraction method

---

```

1  Input:  $P_{T,o}, P_S, P_R, T_m, C_0(z)$ 
2  Recursive computation:
   For  $k = 1, 2, 3, \dots$ 
    $C(z) = C_0(z);$ 
   While True
   (1) Compute the gradient of  $C(z);$ 
   (2) Estimate the incident angle  $\theta_{S,k}$  and  $\theta_{R,k};$ 
   (3) Estimate the travel time  $T_{S,k}$  and  $T_{R,k};$ 
   (4) Estimate the vertically normalized travel time delay  $\delta T_{V,k}$  using Equation (8);
   (5) Estimate the SSVD  $\delta C_k$ 
       If  $\delta T_{V,k} < \gamma$ 
       Break;
       Else if  $\delta T_{V,k} > 0$ 
        $C(z) = \begin{cases} C(z) + \kappa & (z \leq Z_{Surface}) \\ C(z) & (z > Z_{Surface}) \end{cases};$  ( $\kappa$  is a small search step)
       Else
        $C(z) = \begin{cases} C(z) - \kappa & (z \leq Z_{Surface}) \\ C(z) & (z > Z_{Surface}) \end{cases};$ 
       End
    $\delta C_k = C(z) - C_0(z);$ 
   End for

```

Output:  $\delta C$ .

---

Recursions (1)–(3) compute the round-trip travel time based on the classical SRT method. Recursions (4) estimate the vertically normalized travel time delay  $\delta T_{V,k}$  using Equation (8) and the round-trip travel time  $T_m$ . Recursions (5) compute the SSVD  $\delta C_k$  using a small search step to let the  $\delta T_{V,k}$  be close to zero.

### 3.3. Absolute Vertical Position and SSVD Estimation

This study utilizes the numerical optimization iterations approach to estimate the vertical position of a seafloor transponder and SSVD. For previous research, the SSVD are usually reconstructed by a combination of series of the basis function:

$$\delta C_k = \alpha + \sum_i \beta_i \Gamma_i(k) + \eta_i r(k) \cos(\gamma(k) - \gamma_a), \quad (13)$$

where  $\alpha$  is a constant of sound velocity, and  $\beta_i$  and  $\eta_i$  are the coefficients of the basis function.  $\Gamma_i(t)$  represents the basis function with different periods, e.g., second degree polynomial, or quadratic curve,  $r(t)$  is the horizontal distance from transponder to transducer,  $r(k) \cos(\gamma(k))$  indicates the vessel position at time  $t$ , and  $\gamma_a$  represents the horizontal gradient effect.

Considering the complex of the SSVD during the moving survey, in this research, the  $\delta C$  is analyzed by the Empirical Mode Decomposition (EMD) method, as shown in Appendix B, which is a time–frequency analysis method to process non-linear and non-stationary signals [34]. EMD can decompose the  $\delta C$  to a sum of some IMFs  $u_i$  with different periods and residual  $r_m$  adaptively without any prior knowledge.

$$\delta C = \sum_{i=1}^m u_i + r_m, \quad (14)$$

As shown in Figure 5, for estimating the vertical position and SSVD, two kinds of calibration survey line observations are used to estimate the horizontal position and vertical position, respectively. The horizontal position calculated by the circle line is used directly to estimate other unknown parameters. We utilize a certain acoustic velocity structure to estimate the vertical position with the cost function  $J(\delta Z_T, \delta C_{Surface})$ . Then, we recompute the vertically normalized travel time delay.

The SSVD is extracted using the above SRT method. We iterate this process until the position parameters converge.

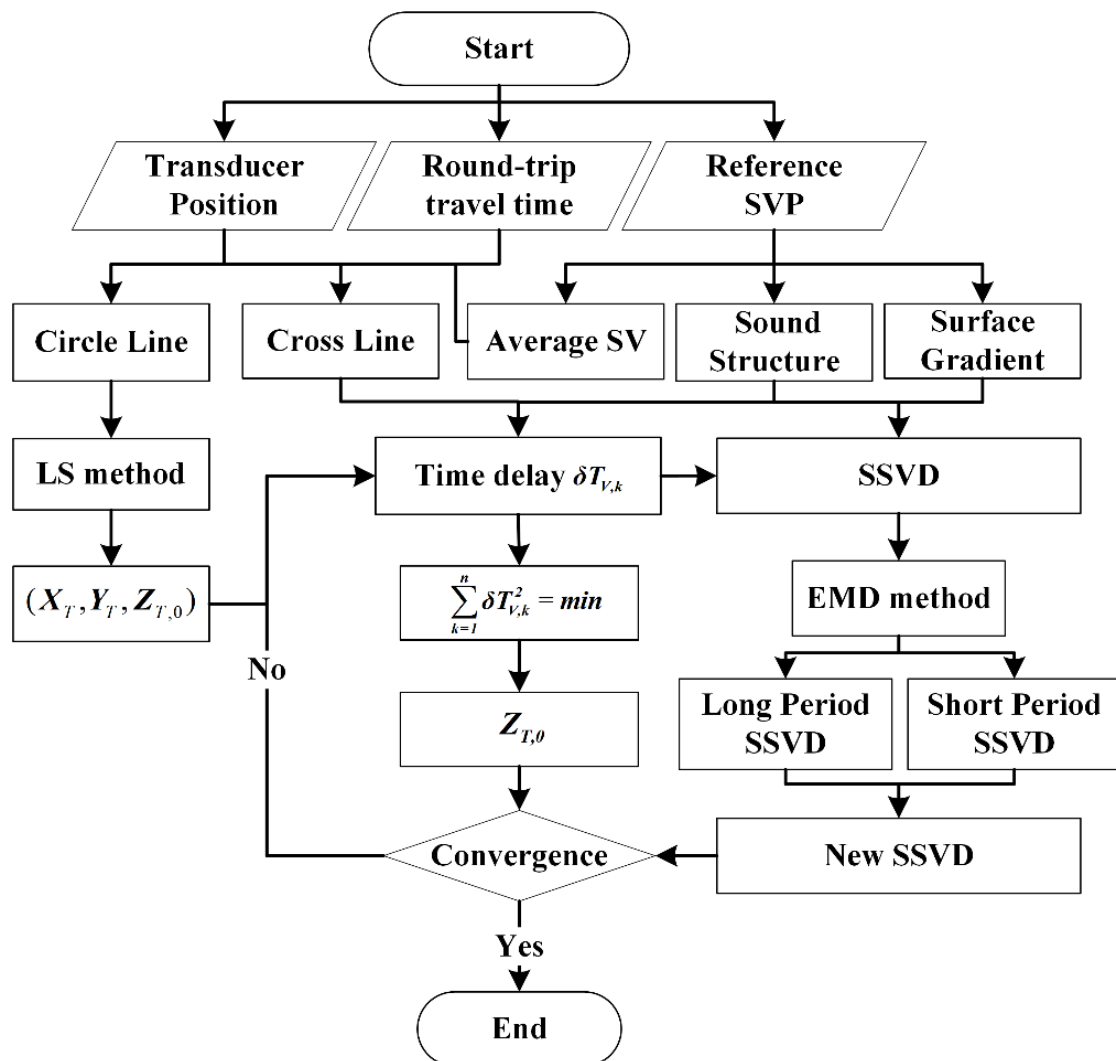


**Figure 5.** Algorithm of parameter estimation used to obtain the absolute vertical position and sound velocity variation.

The EMD method can be utilized to distinguish the effect between the sound velocity variation and the depth error. The surface sound velocity perturbation might have short time periods and long time periods, whereas some previous studies have already proved it [17]. In particular, to distinguish the effect of the vertical basis and the long period disturbance, the relevance index should be computed and adjusted. In our method, the SSVD is decomposed into a sum of different period disturbances, and a new SSVD is reconstructed by combining the long period disturbance and short period disturbance.

#### 4. Experimental Analysis

To analyze the GNSS/Acoustic seafloor geodetic absolute calibration precision, we utilized data from a moving survey calibration experiment in the South China Sea (19°42' N, 115°08' E) with a depth of 1750 m on 3 April 2021, as shown in Figure 6. The raw data mainly included the GNSS observations, ship attitudes, round trip travel times of acoustic signals, GNSS offset from the GNSS antenna to the transceiver and sound velocity profiles. The kinematic GNSS observations were obtained using the Veripos APEX with an approximately horizontal and vertical accuracy 10 and 20 cm, respectively. The attitude of the survey ship was obtained using the POS MV 320 of Applanix company (Richmond Hill, ON, Canada). The acoustic ranging data was obtained using the HiPap

102PMGC of Kongsberg company (Kongsberg, Norway) high precision acoustic positioning system with ultra-long range capabilities (cymbal model) and a cNODE transponder, measuring the travel times of acoustic signals with an approximate range accuracy of 0.02 m. During the trial period, a single transponder was set on the seafloor lander as the entity geodetic station.

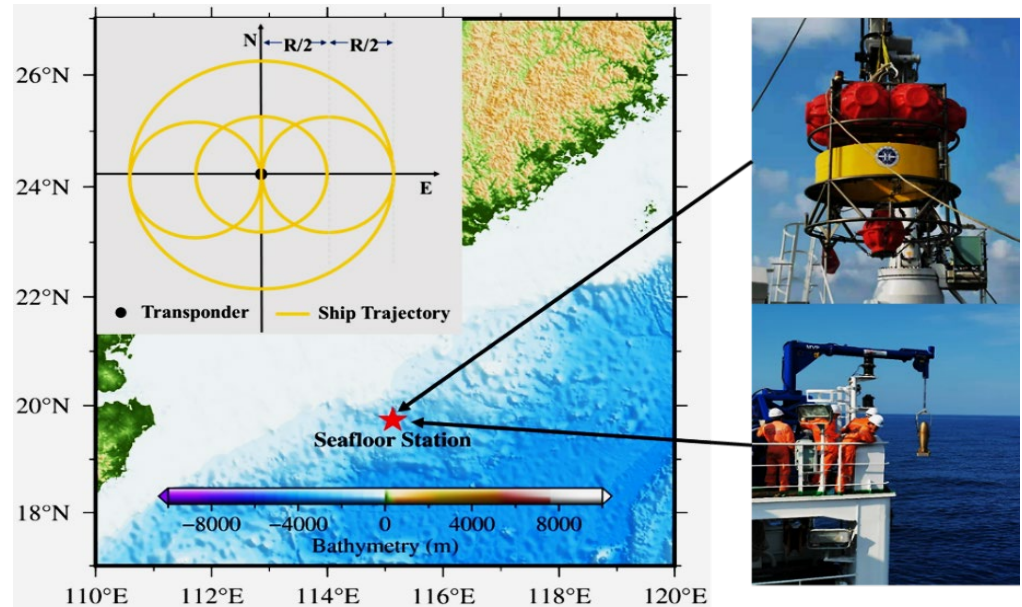


**Figure 6.** The ship trajectory scheme as it collected GNSS/acoustic data with a lander and mobile velocity profile.

After the lander was deployed on the seafloor, the vessel sailed according to the predetermined circle track lines (Figure 7a) and cross track line (Figure 7b) centered on the seafloor station. The number of all acoustic observations was about 5150, and the sampling rate was 4 s. Table 1 shows the data list of acoustic measurements at the seafloor reference points.

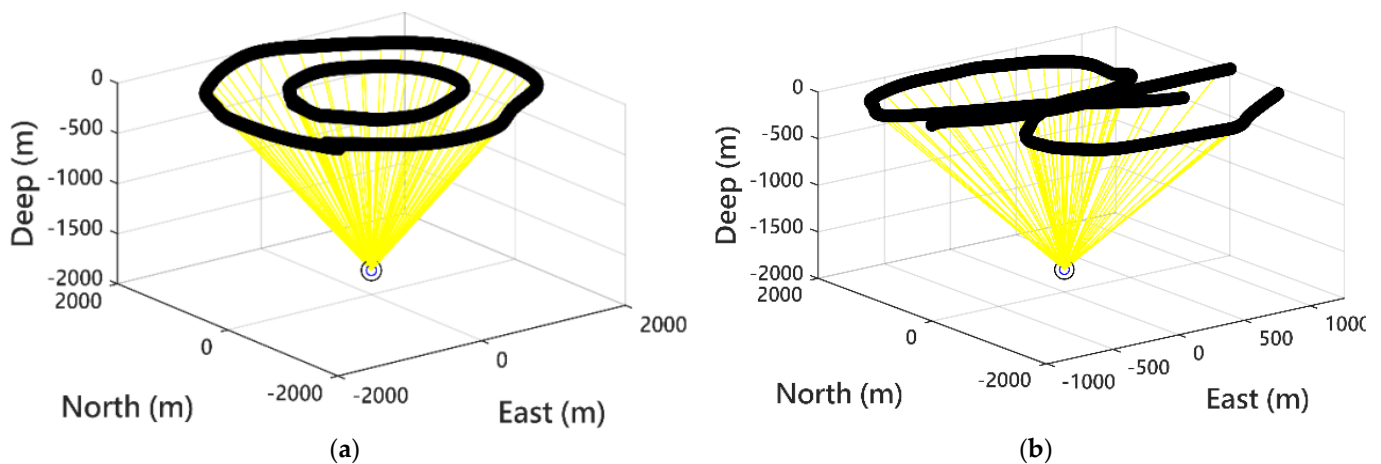


**Figure 7.** Two circles around the seafloor transponder with  $R = 2000$  and  $R = 1000$  (a). A crossing along the diameter directly above the transponder and a figure eight with the seafloor transponder in the center with  $R = 1000$  (b).

**Table 1.** The information of acoustic measurements.

Trajectory	Time First Sample	Time Last Sample	Number of Samples
A circle, $R = 2000$	3 April 2021 04:11	3 April 2021 06:25	2006
A circle, $R = 1000$	3 April 2021 06:43	3 April 2021 08:19	1148
A eight, $R = 1000$	3 April 2021 08:31	3 April 2021 10:27	2004

As shown in Figure 8a, the average incident angles of the big circle and small circle are  $43^\circ$  and  $28^\circ$ . The incident angles of the cross line (eight track) are distributed from  $0^\circ$  to  $45^\circ$ . Three sound velocity profilers in seawater were measured by MVP 300 from the AML Oceanographic company, and the resulting profiles are shown in Figure 8b. The time span of these extracted data was approximately 6 h, ranging from 3:40:00 to 8:20:00 in Coordinated Universal Time (UTC). The average profile of three SVPs is utilized as the reference SVP in this study, and the mean velocity is about 1492 m/s.

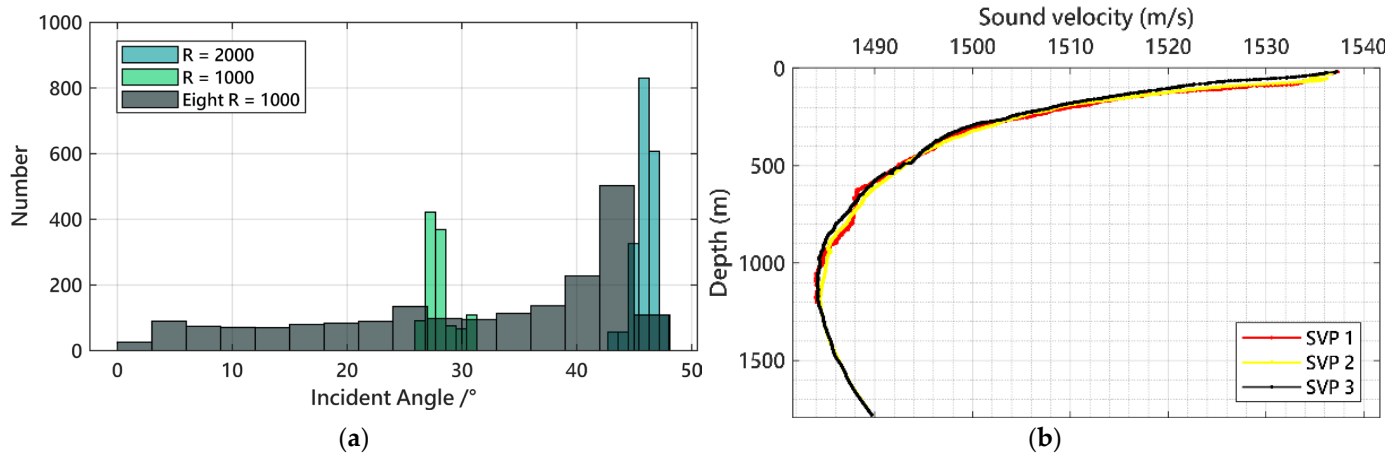


**Figure 8.** The incident histogram of the three trajectories (a). Sound velocity profiles of the water column during the GNSS/Acoustic survey (b).

To estimate the absolute horizontal position of a seafloor transponder, we used the circle line observation. As shown in Figure 9a, the round trip travel times of big circle and small circle track are approximately 3.4 and 2.7 s, respectively. Using the ray-tracing calculations and Equation (7), the travel time delay and horizontal normalized travel time delay can be estimated, as shown in Figure 9b. The root mean square (RMS) values of the travel time delay and horizontal normalized travel time delay are 0.18 and 0.11 ms, respectively.

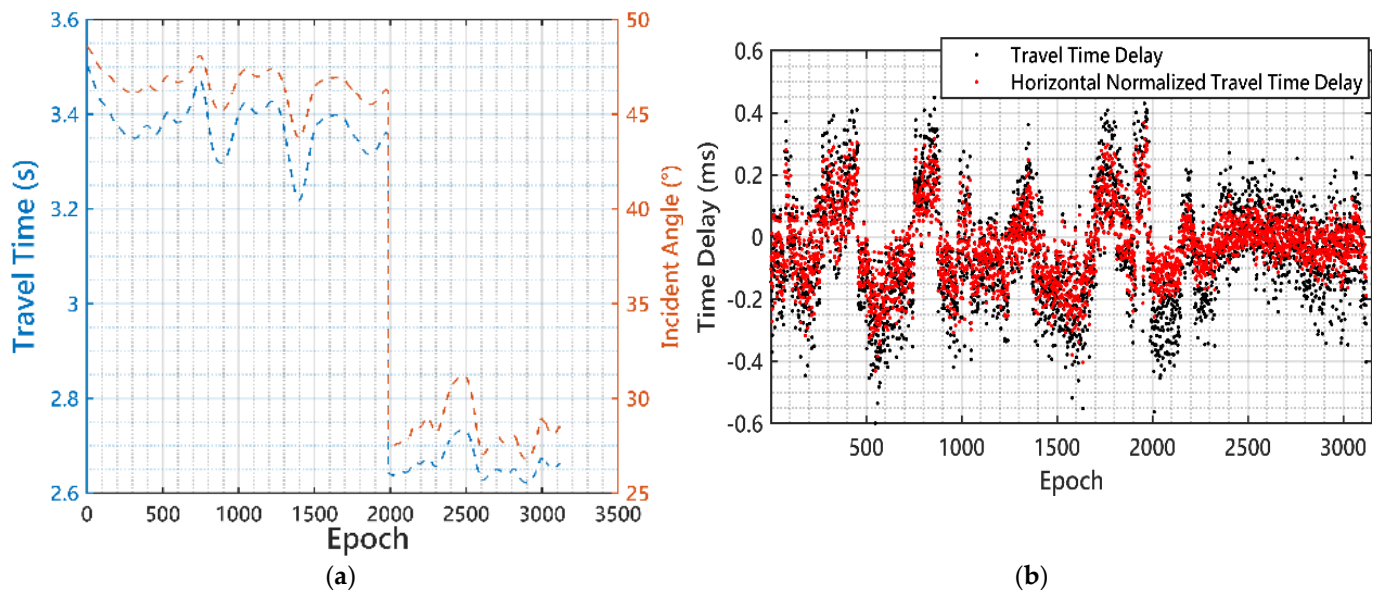


**Figure 9.** The acoustic round-trip travel time and incident angle of the circle line (a). The travel time delay and horizontal normalized travel time delay of the circle line (b).

The travel time delay and horizontal normalized travel time delay are utilized to estimate the horizontal position with LS method, respectively. Figure 10 shows the histogram of acoustic horizontal range residuals for two LS methods. The RMS of the range residuals for travel time delay

and horizontal normalized travel time delay are 13.21 and 8.26 cm, respectively. In addition, the range residuals had mean values of 3.48 and 2.12 cm, respectively. Even though the horizontal range precision in horizontal positioning is limited by systematic errors, the mean value of slant range residuals for the circle line is close to zero. Furthermore, the horizontal position can be utilized to estimate the vertical position and surface sound velocity disturbance.

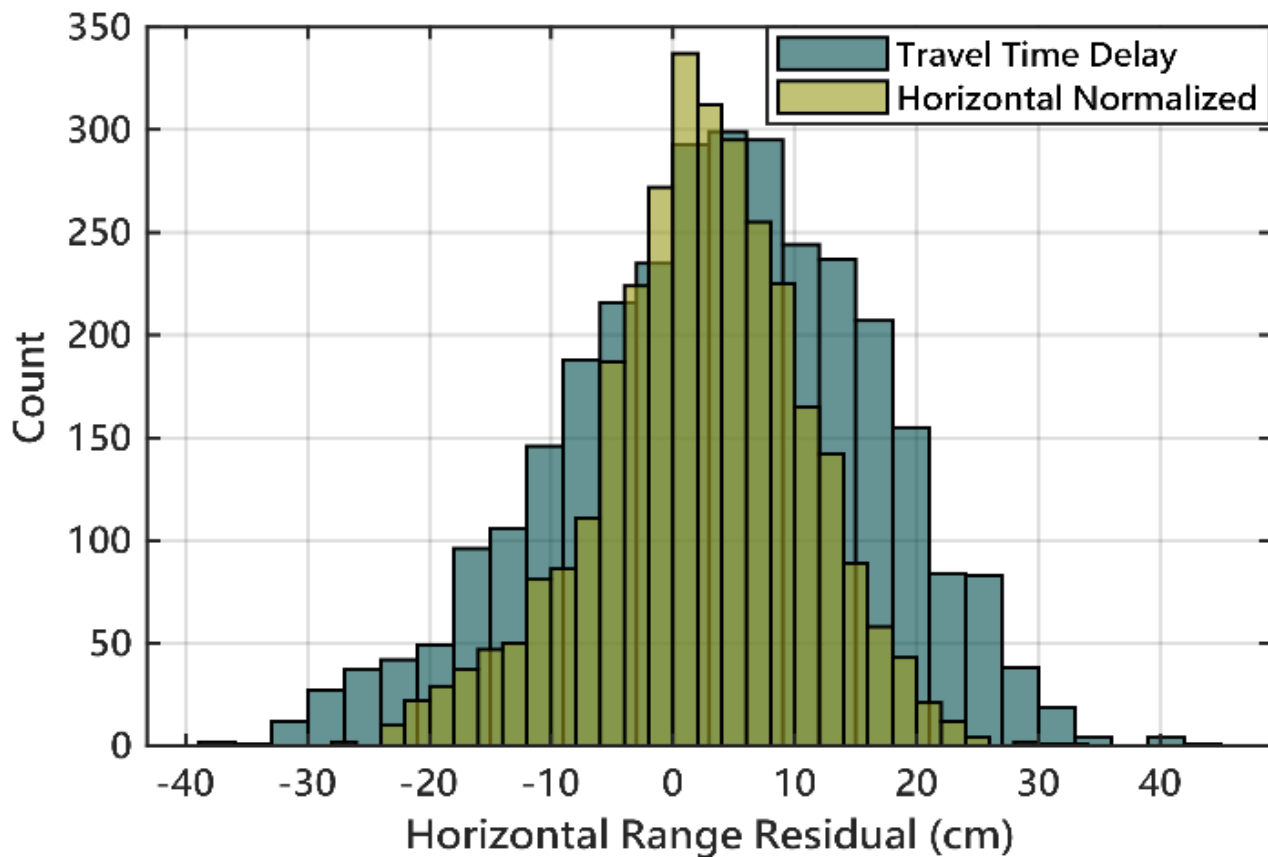


**Figure 10.** The histogram of circle line acoustic horizontal range residuals for the LS method with round-trip travel time delay and horizontal normalized travel time delay.

To estimate the absolute vertical position of a seafloor transponder, we used the cross line observation. As shown in Figure 11a, the round trip travel times vary from 2.3 to 3.3 s. Using the ray-tracing calculations and Equation (8), the travel time delay and vertical normalized travel time delay can be estimated, as shown in Figure 11b. The root mean square (RMS) values of the travel time delay and vertical normalized travel time delay are 0.22 and 0.21 ms, respectively. The mean value of travel time delay and vertical normalized travel time delay are  $-0.83$  and  $-0.68$  ms, respectively. The effect of the delay on the ranging results in an uncertainty of about half a meter in vertical positioning. The IMFs of different periods can be calculated according to the SSVD extraction method in Section 3.2 by setting different surface depths as the initial condition. As shown in Figure 12a, the larger the reference depth is set, the smaller the SSVD value will be. The SSVD can be decomposed with different IMFs, as shown in Figure 12b. Although the amplitude of IMFs is different, the tendency of the IMFs with different reference depths is similar. Considering that the temporal and spatial variation of the surface sound velocity of seawater is more obvious and the variation range is larger, the reference water depth is selected as 300 m in this paper.

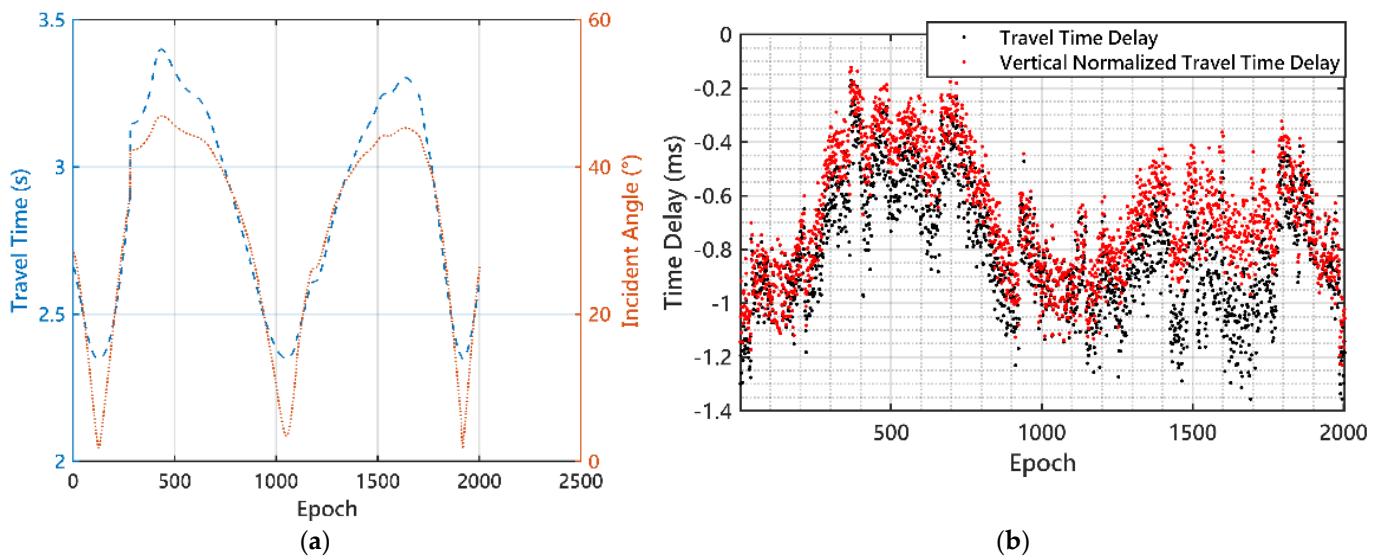


**Figure 11.** The acoustic round-trip travel time and incident angle of the cross line (a). The travel time delay and vertical normalized travel time delay of the cross line (b).

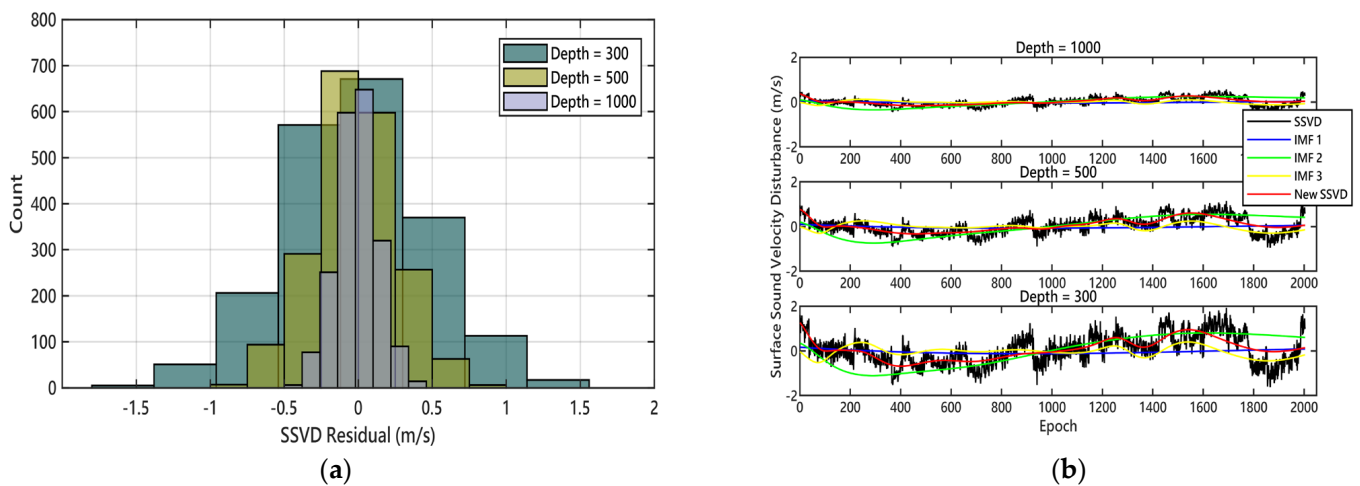


**Figure 12.** The histogram of surface sound velocity disturbance with different surface reference depths (a). The intrinsic mode functions of surface sound velocity disturbance with different reference depth using the IMF method (b).

The vertical position and SSSD can be estimated by the new numerical iterations approach mentioned in Section 3.3. The new SSVD is constructed using IMFs of different cycles and is then used to iteratively calculate the vertical component. As shown in Figure 13a,b, the vertical range residual with different iterations reduced step by step, and the periodic fluctuations associated with SSSD were gradually eliminated.

The LS method, least squares with unknown sound velocity (LS + C) method in which the average bias of sound velocity is regarded as unknown parameters, the SD least squares method, and the new numerical iterations approach were conducted and compared for underwater acoustic positioning. Table 2 presents the residuals statistics of different algorithms for vertical position. For the case of underwater 1750 m depth, the vertical RMS of SD and new method are 18.6 and 7.3 cm compared to the 32.6 cm of LS, with an improvement of 42.9% and 77.6%. The vertical Max and Mean of the new method is significantly better than the other three schemes.

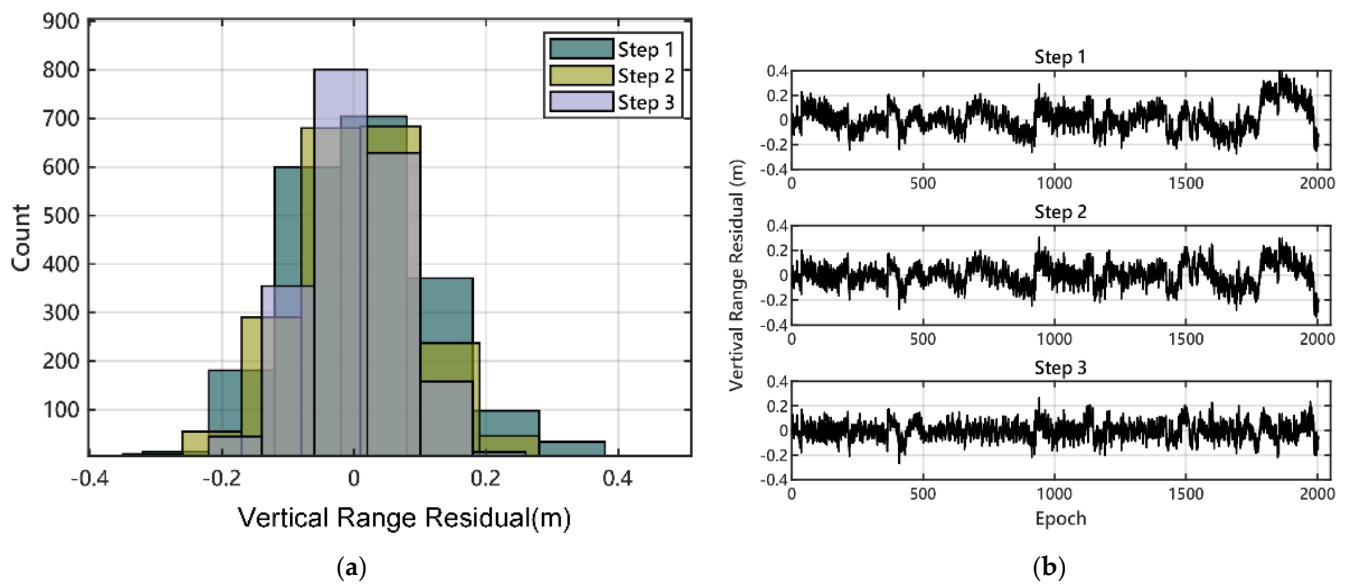


**Figure 13.** The histogram of vertical range residual with different iterations (a). The vertical range residual with different iterations (b).

**Table 2.** The residuals statistics of all methods for vertical position.

Method	RMS (cm)	Max (cm)	Mean ( $ V_V $ ) (cm)
LS	32.6	104.1	25.9
LS + C	26.5	82.2	18.6
SD	18.6	72.8	14.7
New method	7.3	26.7	5.7

## 5. Conclusions

This study presents an approach of correction for vertical position and sound velocity variation on GNSS/Acoustic seafloor geodetic calibration with moving survey data. The horizontal and vertical positions are estimated to utilize a step-by-step method with circle and cross line survey data. After the validation from a real example, the following conclusions can be drawn.

For the horizontal position component, the symmetric circle line reduced the influence of sound velocity errors and ensured the correctness of the horizontal estimation. The horizontal position can be utilized to estimate the vertical position and surface sound velocity disturbance.

To overcome the vertical defects of the GNSS/acoustic technique, the new numerical iterations were studied. We utilize a certain acoustic velocity structure to estimate the vertical position and SSVD with the vertical normalized travel time delay of the cross line. The SSVD is decomposed into a sum of different period disturbances, and a new SSVD is reconstructed by combining the long period disturbance and short period disturbance. The estimation results illustrated that the GNSS/acoustic calibration precision can be improved by implementing the numerical iterations method.

**Author Contributions:** All authors contributed to the study conception and design. Material preparation, data collection, and analysis were performed by R.S., H.L. (Huimin Liu), S.Z., and H.L. (Haojun Li). The first draft of the manuscript was written by R.S. and H.L. (Huimin Liu), and all authors commented on previous versions of the manuscript. All authors have read and agreed to the published version of the manuscript.

**Funding:** The study is funded by the National Natural Science Foundation of China (grant numbers 41406115 and 42174021), National key research and development program of China (grant number 2017YFC0306603), the project of China Geological Survey (grant numbers DD20191003 and DD20221720), and the State Key Laboratory of Geo-Information Engineering (grant number SKLGIE2020-M-1-1).

**Data Availability Statement:** All data included in this study are available upon reasonable request from the corresponding author.

**Acknowledgments:** The authors would like to thank China University of Petroleum (East China) for providing the basis code of the sound ray tracing method. The authors also thank the editor and reviewers for their comments and suggestions, which greatly improved the content of this article.

**Conflicts of Interest:** The authors declare no conflict of interest.

## Appendix A

When the average sound velocity along the actual ray path is expressed as  $C_m$ , the Euclidean distances between the transceiver and the transponder are calculated as follows:

$$C_m T_{m,k} = \rho_{S,k} + \rho_{R,k} + \Delta\rho_{C,k} + \omega_k \quad (A1)$$

$$= \sqrt{(x_T - x_{S,k})^2 + (y_T - y_{S,k})^2 + (z_T - z_{S,k})^2} + \sqrt{(x_T - x_{R,k})^2 + (y_T - y_{R,k})^2 + (z_T - z_{R,k})^2} + \Delta\rho_{C,k} + \omega_k$$

where  $\delta c$  is the sound velocity perturbation,  $\Delta\rho_{C,k} = (T_{S,k} + T_{R,k})\delta c$  is the sound velocity error and  $\omega_k$  represents the random error. By linearizing Equation (A1), the error equation of round-trip range observation can be represented as follows:

$$v_k = \mathbf{a}_k \cdot \delta P_T - (C_m T_{m,k} - \rho_{o,k} - \Delta\rho_k) \quad (A2)$$

$$\rho_{o,k} = \sqrt{(x_{T,o} - x_{S,k})^2 + (y_{T,o} - y_{S,k})^2 + (z_{T,o} - z_{S,k})^2} + \sqrt{(x_{T,o} - x_{R,k})^2 + (y_{T,o} - y_{R,k})^2 + (z_{T,o} - z_{R,k})^2} \quad (A3)$$

$$\mathbf{a}_k = [\sin\theta_{S,k} \cos\gamma_{S,k} + \sin\theta_{R,k} \cos\gamma_{R,k} \quad \sin\theta_{S,k} \sin\gamma_{S,k} + \sin\theta_{R,k} \sin\gamma_{R,k} \quad \cos\theta_{R,k} + \cos\theta_{S,k}] \quad (A4)$$

where  $\mathbf{a}_k$  denotes the partial derivatives of the distance function with respect to the unknown position parameters.  $\gamma_{S,k}$  and  $\gamma_{R,k}$  are represented as the sending and receiving azimuth angle, respectively.

As shown in Figure 2b, if the sound velocity error  $\Delta\rho_{C,k}$  is negligible, based on Equation (A2) and the least-squares methods, the correction of  $\delta P_T$  can be estimated as follows:

$$\delta P_T = (\mathbf{A}^T \mathbf{A})^{-1} \mathbf{A}^T \mathbf{L} \quad (A5)$$

where  $\mathbf{A} = [\mathbf{a}_1^T \quad \mathbf{a}_2^T \quad \dots \quad \mathbf{a}_n^T]^T$ ,  $\mathbf{L} = [v_1^T \quad v_2^T \quad \dots \quad v_n^T]^T$ .

## Appendix B

With respect to the Empirical Mode Decomposition (EMD), signals can be decomposed as Intrinsic Mode Functions (IMFs) subjected to the following conditions:

(1) In the whole data set, the number of extrema and the number of zero crossing must either equal or differ at most by one;

(2) At any data point, the mean value of the envelope defined using the local maxima and the envelope defined using the local minima is zero.

The decomposition of one-dimensional signal can be presented as:

$$x(t) = \sum_{i=1}^n imf_i(t) + r_n(t) \quad (A6)$$

where  $imf_i(t)$  stands for intrinsic model functions, and  $r_n(t)$  stands for the monotonic residual functions.

The EMD algorithm is accomplished through a sifting process, and the main process is as follows:

Step 1: calculate the extrema of signal  $x(t)$ ;

Step 2: calculate the envelopes  $e_{\min}(t)$  and  $e_{\max}(t)$  corresponding to the minima and maxima, respectively;

Step 3: calculate the mean value of envelopes  $m(t) = (e_{\min}(t) + e_{\max}(t))/2$ ;

Step 4: extract the details  $d(t) = x(t) - m(t)$ ;

Step 5: repeat Steps 1–4 to extract details until the mean value of  $d(t)$  is zero, and then this  $d(t)$  is regarded as one IMF;

Step 6: calculate the residual  $r(t) = x(t) - imf_i(t)$ ;

Step 7: repeat the following steps until there are no IMFs in the residual, and the decomposition process of EMD has been finished thus far.

## References

1. Spiess, F.N. Suboceanic geodetic measurements. *IEEE Trans Geosci. Remote Sens.* **1985**, *23*, 2–510. [[CrossRef](#)]
2. Gagnon, K.L.; Chadwell, C.D. Relocation of a seafloor transponder—sustaining the GPS-acoustic technique. *Earth Planets Space* **2007**, *59*, 327–336. [[CrossRef](#)]
3. Yokota, Y.; Ishikawa, T.; Watanabe, S.; Tashiro, T.; Asada, A. Seafloor geodetic constraints on interplate coupling of the Nankai Trough megathrust zone. *Nature* **2016**, *534*, 374–377. [[CrossRef](#)] [[PubMed](#)]
4. Sato, M.; Fujita, M.; Matsumoto, Y.; Ishikawa, T.; Asakura, T. Improvement of GPS/acoustic seafloor positioning precision through controlling the ship's track line. *J. Geod.* **2013**, *87*, 825–842. [[CrossRef](#)]
5. Kido, M.; Fujimoto, H.; Hino, R.; Ohta, Y.; Osada, Y.; Iinuma, T.; Azuma, R.; Wada, I.; Miura, S.; Suzuki, S.; et al. Progress in the project for development of GPS/acoustic technique over the last 4 years. In *International Symposium on Geodesy for Earthquake and natural Hazards (GENAH)*; Hashimoto, M., Ed.; Springer: Cham, Switzerland, 2015; Volume 145.
6. Fujimoto, H. Seafloor geodetic approaches to subduction thrust earthquakes. *Monogr. Environ. Earth Planets* **2014**, *2*, 23–63. [[CrossRef](#)]
7. Honscho, C.; Kido, M.; Tomita, F.; Uchida, N. Offshore postseismic deformation of the 2011 Tohoku earthquake revisited: Application of an improved GPS-acoustic positioning method considering horizontal gradient of sound velocity structure. *J. Geophys. Res. Solid Earth* **2019**, *124*, 5990–6009. [[CrossRef](#)]
8. Sweeney, A.D.; Chadwell, C.D.; Hildebrand, J.A.; Spiess, F.N. Centimeter-Level Positioning of Seafloor Acoustic Transponders from a Deeply-Towed Interrogator. *Mar. Geod.* **2005**, *28*, 39–70. [[CrossRef](#)]
9. Chadwell, C.D.; Spiess, F.N. Plate motion at the ridge-transform boundary of the south Cleft segment of the Juan de Fuca Ridge from GPS-Acoustic data. *J. Geophys. Res. Solid Earth* **2008**, *113*, B04415. [[CrossRef](#)]
10. Ikuta, R.; Tadokoro, K.; Ando, M.; Okuda, T.; Sugimoto, S.; Takatani, K.; Yada, K.; Besana, G.M. A new GPS-acoustic method for measuring ocean floor crustal deformation: Application to the Nankai Trough. *J. Geophys. Res.* **2008**, *113*, B02401. [[CrossRef](#)]
11. Spiess, F.N.; Chadwell, C.D.; Hildebrand, J.A.; Young, L.E.; Purcell, G.H.; Dragert, H. Precise GPS/Acoustic positioning of seafloor reference points for tectonic studies. *Phys. Earth Planet. Inter.* **1998**, *108*, 101–112. [[CrossRef](#)]
12. Asada, A.; Yabuki, T. Centimeter-level positioning on the seafloor. *Proc. Jpn. Acad. Ser. B Phys. Biol.* **2017**, *77*, 7–12. [[CrossRef](#)]
13. Xu, P.; Ando, M.; Tadokoro, K. Precise, three-dimensional seafloor geodetic deformation measurements using difference techniques. *Earth Planets Space* **2005**, *57*, 795–808. [[CrossRef](#)]
14. Fujita, M.; Ishikawa, T.; Mochizuki, M.; Sato, M.; Toyama, S.; Katayama, M. GPS/Acoustic seafloor geodetic observation: Method of data analysis and its application. *Earth Planets Space* **2006**, *58*, 265–275. [[CrossRef](#)]
15. Chadwell, C.D.; Sweeney, A.D. Acoustic ray-trace equations for seafloor geodesy. *Mar. Geod.* **2010**, *33*, 164–186. [[CrossRef](#)]
16. Yang, F.; Lu, X.; Li, J.; Han, L.; Zheng, Z. Precise positioning of underwater static objects without sound velocity profile. *Mar. Geod.* **2011**, *34*, 138–151. [[CrossRef](#)]
17. Yokota, Y.; Ishikawa, T.; Watanabe, S. Gradient field of undersea sound speed structure extracted from the GNSS-A oceanography. *Mar. Geophys. Res.* **2019**, *40*, 493–504. [[CrossRef](#)]
18. Yang, Y.; Xu, T.; Xue, S. Progresses and prospects in developing marine geodetic datum and marine navigation of China. *Acta Geod. Et Cartogr. Sin.* **2017**, *46*, 1–8.
19. Yang, Y.; Liu, Y.; Sun, D.; Xu, T.; Xue, S.; Han, Y.; Zeng, A. Seafloor geodetic network establishment and key technologies. *Sci. China Earth Sci.* **2020**, *63*, 1188–1198. [[CrossRef](#)]
20. Chen, H.H.; Wang, C.C. Optimal localization of a seafloor transponder in shallow water using acoustic ranging and GPS observations. *Ocean. Eng.* **2007**, *34*, 2385–2399. [[CrossRef](#)]
21. Ballu, V.; Bouin, M.N.; Calmant, S.; Folcher, E.; Bore, J.M.; Ammann, J.; Pot, O.; Diament, M.; Pelletier, B. Absolute seafloor vertical positioning using combined pressure gauge and kinematic GPS data. *J. Geod.* **2010**, *84*, 65–77. [[CrossRef](#)]
22. Osada, Y.; Fujimoto, H.; Miura, S.; Sweeney, A.; Kanazawa, T.; Nakao, S.; Chadwell, C.D. Estimation and correction for the effect of sound velocity variation on GPS/Acoustic seafloor positioning: An experiment off Hawaii Island. *Earth Planets Space* **2003**, *55*, 17–20. [[CrossRef](#)]
23. Kido, M.; Osada, Y.; Fujimoto, H. Temporal variation of sound velocity in ocean: A comparison between GPS/acoustic and in situ measurements. *Earth Planets Space* **2008**, *60*, 229–234. [[CrossRef](#)]
24. Honscho, C.; Kido, M. Comprehensive analysis of traveltime data collected through GPS-acoustic observation of seafloor crustal movements. *J. Geophys. Res. Solid Earth* **2017**, *122*, 8583–8599. [[CrossRef](#)]
25. Watanabe, S.; Ishikawa, T.; Yokota, Y.; Nakamura, Y. GARPOS: Analysis Software for the GNSS-A Seafloor Positioning with Simultaneous Estimation of Sound Velocity Structure. *Front. Earth Sci.* **2020**, *8*, 597532. [[CrossRef](#)]
26. Chen, H.H.; Wang, C.C. Accuracy assessment of GPS/Acoustic positioning using a Seafloor Acoustic Transponder System. *Ocean. Eng.* **2011**, *38*, 1472–1479. [[CrossRef](#)]
27. Yamada, T.; Ando, M.; Tadokoro, K.; Sato, K.; Okuda, T.; Oike, K. Error evaluation in acoustic positioning of a single transponder for seafloor crustal deformation measurements. *Earth Planets Space* **2002**, *54*, 871–881. [[CrossRef](#)]
28. Zhao, J.; Zhou, Y.; Zhang, H.; Wu, Y.; Fang, S. A new method for absolute datum transfer in seafloor control network measurement. *J. Mar. Sci. Technol.* **2016**, *21*, 216–226. [[CrossRef](#)]
29. Chen, G.; Liu, Y.; Liu, Y.; Liu, J. Improving GNSS-acoustic positioning by optimizing the ship's track lines and observation combinations. *J. Geod.* **2020**, *94*, 61. [[CrossRef](#)]

30. Zhao, S.; Wang, Z.; Nie, Z.; He, K.; Ding, N. Investigation on total adjustment of the transducer and seafloor transponder for GNSS/Acoustic precise underwater point positioning. *Ocean. Eng.* **2021**, *221*, 108533. [[CrossRef](#)]
31. Nakamura, Y.; Yokota, Y.; Ishikawa, T.; Watanabe, S. Optimal Transponder Array and Survey Line Configurations for GNSS-A Observation Evaluated by Numerical Simulation. *Front. Earth Sci.* **2021**, *9*, 600993. [[CrossRef](#)]
32. Leonard, J.J.; Bahr, A. Autonomous underwater vehicle navigation. In *Springer Handbook of Ocean Engineering*, 1st ed.; Dhanak, M.R., Xiros, N.I., Eds.; Springer: New York, NY, USA, 2016; pp. 341–357.
33. Tomita, F.; Kido, M.; Honsho, C.; Matsui, R. Development of a kinematic GNSS-Acoustic positioning method based on a state-space model. *Earth Planets Space* **2019**, *71*, 102. [[CrossRef](#)]
34. Huang, N.E.; Wu, Z. A review on Hilbert-Huang transform: Method and its applications to geophysical studies. *Rev. Geophys.* **2008**, *46*. [[CrossRef](#)]